Large magnetoresistance in antiferromagnetic $CaMnO_{3-\delta}$

Z. Zeng and M. Greenblatt*
Department of Chemistry, Rutgers, The State University of New Jersey, Piscataway, New Jersey 08854-8087

M. Croft
Department of Physics, Rutgers, The State University of New Jersey, Piscataway, New Jersey 08854-8019
(Received 22 October 1998)

$CaMnO_{3-\delta}$ with $\delta=0$, 0.06, and 0.11 was prepared by the Pechini citrate gel process at 1100 °C. Oxygen defects were created by quenching the sample from high temperature. Chemical analysis and x-ray absorption show that the formal valence of Mn in $CaMnO_3$ is close to 4+, and that Mn(III) is created in the quenched samples. Moreover the x-ray absorption near-edge spectra results support the creation of two Mn(III) five coordinate sites for each O vacancy. $CaMnO_{3-\delta}$ ($\delta=0-0.11$) are *n*-type semiconductors and order antiferromagnetically with Néel temperatures close to 125 K. The activation energy decreases with increasing δ. A relatively large (~40%) negative magnetoresistance (MR) is observed for $CaMnO_{2.89}$. This result shows that a substantial MR can occur in these *G*-type antiferromagnetic materials. [S0163-1829(99)02913-6]

INTRODUCTION

Recently, magnetoresistance materials have attracted much attention both because of their interesting fundamental structural, electronic, and magnetic properties and their potential application for magnetic recording and sensing.[1–5] By far the $La_{1-x}M_xMnO_3$ ($M=$Ba, Sr, Ca, Pb) system has been studied in the greatest detail.[6–9] Three types of the magnetic structures have been established in this system: $LaMnO_3$ orders antiferromagnetically (AF) with an ''*A*-type'' perovskite structure, where the Mn(III) ions order ferromagnetically (FM) in planes and AF between planes; $La_{1-x}Ca_xMnO_3$ ($0.1<x<0.5$) orders FM with a ''*B*-type'' structure, while in $CaMnO_3$ neighboring Mn(IV) ions order AF with a ''*G*-type'' structure.[10] $LaMnO_3$ has been studied in great detail.[11,12] The formal valence of Mn is near 3+ for the stoichiometric compound. However, part of the Mn(III) can be oxidized to Mn(IV) under suitable conditions due to either or both Ln and/or Mn cation deficiency. This leads to Mn(III)-O-Mn(IV) double exchange interactions and $La_{1-x}Mn_{1-y}O_3$ shows a semiconductor-to-metal transition (SM) at ~200 K with colossal magnetoresistance (CMR) near the SM transition temperature.[13,14] In $CaMnO_{3-\delta}$, the other end of $La_{1-x}Ca_xMnO_3$ system, the formal valence of Mn is near $4+(\delta\sim0)$. Mn(III) should be created in this compound when oxygen defects are introduced (i.e., $\delta>0$). The introduction of Mn(III)-O-Mn(IV) moiety would be expected to decrease the resistivity of the compound, and may lead to double exchange (DE) interactions. In contrast with the hole doped cation-defect $La_{1-x}Mn_xO_3$, oxygen-defect $CaMnO_{3-\delta}$ is electron doped with a ''*G*-type'' magnetic structure. Several groups[15,16] have investigated the electrical resistance and the magnetic properties of $CaMnO_{3-\delta}$, however, magnetoresistance (MR) of $CaMnO_{3-\delta}$ has not been demonstrated thus far. In this paper, we report the x-ray absorption near-edge spectra (XAS), electrical, magnetic, and magnetoresistance properties of $CaMnO_{3-\delta}$ with $\delta=0$, 0.06, 0.11. Comparing the properties of *A*- and *G*-type manganites, we may shed some light on the mechanism of GMR and CMR materials.

EXPERIMENTAL

$CaMnO_{3-\delta}$ was prepared by a sol-gel method. $Mn(NO_3)_2$ was purchased as a 49.7% w/w aqueous solution (Aldrich). Appropriate stoichiometries of $Mn(NO_3)_2$ and $CaCO_3$ (Aldrich, 99+%) were dissolved in an excess amount of 35% nitric acid. An excess of citric acid and ethylene glycol were also added to the solution. The solution was slowly evaporated to a resin and dried. The sample was then heated slowly to 600 °C to decompose the organic compounds, and pressed into pellets at 1 Kbar. The $\delta=0$ material was sintered in flowing oxygen at 1100 °C for 24 h, and then slowly cooled to room temperature. The oxygen-deficient samples were heated in air to 1100 °C for 24 h and then quenched from 1100 or 1000 °C to room temperature.

The powder x-ray diffraction (PXD) data were collected with a SCINTAG PAD V diffractometer with monochromatized CuK_α radiation. Silicon powder was used as an internal standard. Lattice parameters were refined by a least-square method. The dc electrical resistivity and the magnetoresistance measurements were carried out by a standard four-probe technique from 400 to 4 K in a superconducting quantum interference device (SQUID) magnetometer (MPMS, Quantum Design). Magnetic properties were also measured with this SQUID magnetometer in the temperature range 4–400 K.

The Mn *K*-edge XAS measurements were performed on beam lines *X*-19*A* and *X*-18*B* at the Brookhaven National Synchrotron Light Source using a double crystal Si (311) and channel cut Si (111) monochromator, respectively. Electron yield, fluorescence mode, and transmission mode measurements were made and checked for consistency. A standard was run simultaneously with all the measurements for precise calibration. The relative energies between various spectra were established by careful comparison of the standard spectra. In general the relative accuracy of the energy is

TABLE I. Oxidation state and lattice parameters for $CaMnO_{3-\delta}$.

Composition	T_q (°C)[a]	Mn valence	a (Å)	b (Å)	c (Å)	V (Å^3)
$CaMnO_3$	No quench	3.99	5.2641(3)	5.2782(2)	7.4546(1)	207.13(2)
$CaMnO_{2.94}$	1000	3.88	5.2647(3)	5.2792(2)	7.4601(1)	207.34(2)
$CaMnO_{2.89}$	1100	3.78	5.2644(1)	5.2802(1)	7.4622(2)	207.42(1)

[a]T_q temperature of quenching.

about ± 0.05 eV.[17] All spectra were normalized to unity step in the absorption coefficient from well below to well above the edge.

Chemical analysis were made with a Baird Atomic Model 2070 inductively coupled plasma emission spectrometer (ICP). The oxidation state of Mn was determined by a chemical titration in which the samples were dissolved in dilute sulfuric and phosphoric acids with an excess of $Fe(NH_4)_2(SO_4)_2$, and titrated with $KMnO_4$ solution.

RESULTS AND DISCUSSIONS

Oxidation State of Mn. Chemical titration shows that the formal oxidation state of Mn is near 4+ for the sample prepared in oxygen atmosphere (Table I). The formal oxidation state of Mn decreases with increasing temperature of quenching. The results of the titration measurements can be interpreted in terms of the titration-Mn-valence v_t(Mn) and/or the O-vacancy content δ (i.e., $CaMnO_{3-\delta}$) with $v_t(\mathrm{Mn}) = 4 - 2\delta$. For the O_2 prepared and 1100 °C quenched materials values of $\delta = 0/v_t(\mathrm{Mn}) = 3.99$ and $\delta = 0.11/v_t(\mathrm{Mn}) = 3.78$ were found. Thus the titration results indicate that about 20% of the Mn sites are reduced to Mn(III) in the $CaMnO_{3-\delta}$ ($\delta = 0.11$) material. The results of the Mn-K XAS, below, support the formation of two Mn(III) sites associated with each of these O defects.

The Mn-K edges of the $CaMnO_{3-\delta}$ with $\delta = 0$ and $\delta = 0.11$ along with that of the Mn(III) compound $LaMnO_3$, are shown in Fig. 1. The most intense B feature at these edges is related to $1s$-to-$4p$ transitions. The systematic upshift of this feature with increasing Mn valence has been well established in studies of the $La_{1-x}Ca_xMnO_3$ system (illustrated in Fig. 2 by the end point spectra).[17] Comparing the $CaMnO_{3-\delta}$ ($\delta = 0.11$) spectrum with that of $CaMnO_3$ one notes that, although their B features peak at the same energy, there is substantial excess intensity in the O-deficient spectrum on the low-energy side of the B peak. Indeed the placement of the excess intensity is suggestive of a new component in the spectrum with a B feature close to that of $LaMnO_3$.

The presence of an O vacancy, at the shared corners of adjacent Mn octahedra, would be expected to induce two adjacent Mn(III) sites into the Mn(IV) lattice of $CaMnO_3$. With this in mind, one can extract an estimate of the Mn-defect site spectral component by assuming that the ~80% Mn(IV) component of the spectrum is unchanged from that of the fully oxidized $CaMnO_3$. [Note the 22% Mn(III) concentration has been rounded to 20% since the method is only approximate.] The approximation of the defect-site (DS) spectrum, by a weighted, renormalized difference spectrum, is shown in Fig. 1. One should note that the peak of the DS-difference spectrum is at the same energy as that of the Mn(III)-$LaMnO_3$ spectrum. The additional structure on the low-energy side of the difference spectrum (in the energy range labeled A) is not unreasonable in view of the distorted five-coordinate defect environment. Such a distorted environment typically leads to splittings in the $4p$ features at the K edges of transition metals.[18,19] This identification of a distinct Mn(III) site spectral component in the Mn(IV) background stands in contrast to the $La_{1-x}Ca_xMnO_3$ system where a continuous shift of the Mn-K edge spectra from Mn(IV) to Mn(III) was observed.[17]

Before discussing the expanded-energy-scale pre-edge a feature, it is worth noting the behavior of the D^* feature, shown in Fig. 1. In the previous XAS study of the $La_{1-x}Ca_xMnO_3$ system this D^* feature is systematically enhanced with increasing Mn valence. However, discussion of this D^* feature was omitted in the previous work.[17] In Fig. 1 the D^* feature can be seen to be degraded with O deficiency, and this is again consistent with the reduction of the Mn(IV) content.

Figure 2 shows an expanded view of the pre-edge spectra, i.e., the region labeled (a) in Fig. 1. Comparison of the $CaMnO_{3-\delta}$, $\delta = 0$ and $\delta = 0.11$ spectra clearly shows that a substantial decrease of the a-feature resolution and spectral weight accompanies the increased O deficiency. (The larger absolute magnitude of the spectral intensity in the a-feature region of the $\delta = 0.11$ curve is due to the much larger back-

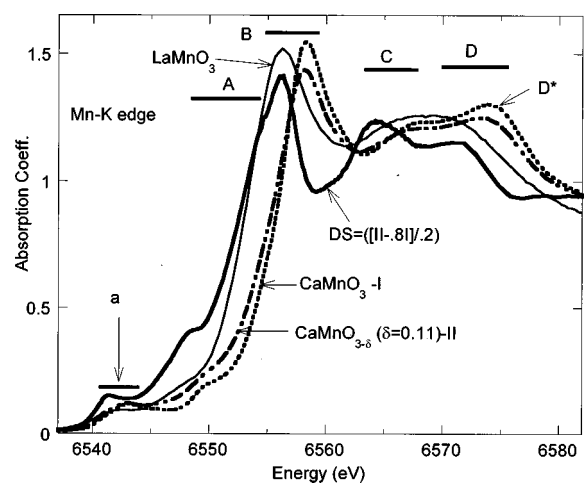

FIG. 1. Mn-K edge for the Mn(III) perovskite $LaMnO_3$, the fully oxygenated Mn(IV) perovskite $CaMnO_3$ (referred to as I), and the oxygen deficient $CaMnO_{3-\delta}$ ($\delta = 0.11$) (referred to as II). Motivated by the titration results, which estimate that about 20% of the Mn sites may be reduced to Mn(III) in the $CaMnO_{3-\delta}$ ($\delta = 0.11$) material, the defect site (DS) difference spectrum [(II-0.8I)/0.2] was plotted. Also the disparity between $\delta = 0.11$ (~22% reduction) and the 20% reduction is neglected due to the approximate nature of the difference spectrum calculation.

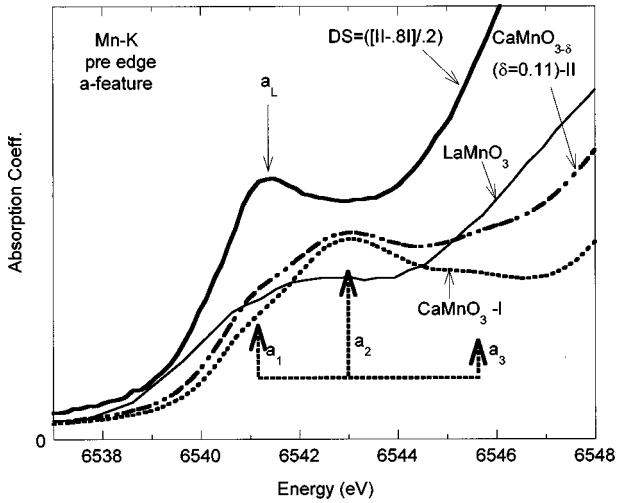

FIG. 2. Mn-K pre edge for the Mn(III) perovskite $LaMnO_3$, the fully oxygenated Mn(IV) perovskite $CaMnO_3$ (I), and the oxygen deficient $CaMnO_{3-\delta}$ ($\delta=0.11$) (II). The DS difference spectrum [(II-0.8I)/0.2] estimate is as discussed above. The three components a_1, a_2, and a_3 of the $CaMnO_3$ pre-edge should be noted.

ground.) In view of the established increased a-feature intensity with increasing Mn valence,[17] these observations are again consistent with the reduction of Mn(IV) to Mn(III) upon O depletion.

Inspection of Fig. 2 also reveals a distinct change in the a-feature energy distribution in these materials. The Mn(IV)-$CaMnO_{3-\delta}$, $\delta=0$ a feature can be seen to contain three identifiable subfeatures a_1, a_2, and a_3. (Previous, lower resolution work only identified the a_1 and a_2 features.[17]) The Mn(III)-$LaMnO_3$ a feature consists of a broad, much weaker, and apparently unresolved bimodal structure. The $LaMnO_3$, a-feature onset also has a modest but distinct shift to lower energy relative to the $CaMnO_3$ a-feature onset. The DS-difference spectrum, in Fig. 2, manifests this same distinct shift to lower energy, characteristic of the Mn(III) character of the defect induced sites. Interestingly the DS also shows a quite robust peak (labeled a_L). The enhancement of this a_L-feature intensity (relative to that of $LaMnO_3$) is consistent with the square-pyramidal environment at the defect sites.[20] Namely, the enhancement of the p/d admixture in such noncentrosymmetric sites has been established to consistently enhance such transition metal pre-edge features.[21]

Thus both the main- and pre-edge XAS results provide evidence of Mn(III) behavior for the defect sites in the $CaMnO_{3-\delta}$, system. As noted, this stands in contrast to the behavior of the $La_{1-x}Ca_xMnO_{3-\delta}$, Mn-$K$ XAS results where distinct site behavior was not discernible.[17] Interestingly, structural studies have shown that the highly O-deficient $CaMnO_{3-\delta}$, $\delta=0.5$ material forms a structure where all sites are equivalent with this five coordination.[20] Studies of the crossover to this ordered structure should be quite interesting and are being pursued. It is worth noting that the O-defect structure in this system stands in contrast to that in the $SrCoO_{3-\delta}$ system where the $\delta=0.5$ material forms the Brownmillerite structure. Indeed Co-K XAS studies show the segregation of four-coordinated Co(II)-O defect and six-coordinated Co(IV)-O sites in this Co case.[22]

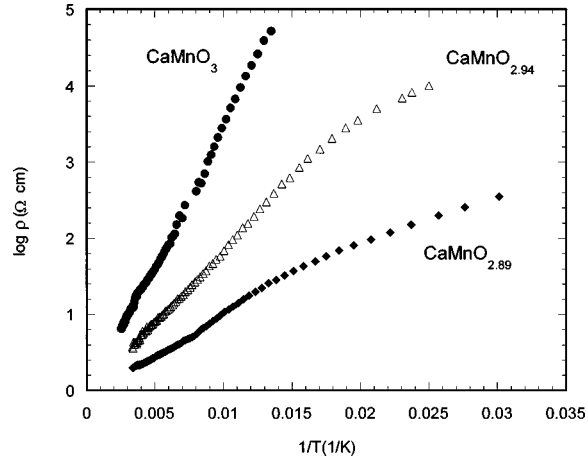

FIG. 3. $\log_{10}\rho$ vs $1/T$ for $CaMnO_{3-\delta}$.

Lattice parameters. $CaMnO_{3-\delta}$ crystallizes in orthorhombic perovskite structure in space group P_{nma}.[20] The unit cell parameter c and the volume increase with increasing quenching temperature, and hence δ (see Table I). This is consistent with the increase of Mn(III) content and the increased effective ionic radius of Mn(III) (0.72 Å) relative to that of Mn(IV) (0.67 Å).[23]

Electronic properties. Figure 3 shows the variation of $\log_{10}\rho$ with $1/T$ for $CaMnO_{3-\delta}$. All the compounds are semiconducting. Qualitative Seebeck measurements for these samples show n-type behavior. The electrical conductivity increases and the activation energy decreases with decreasing oxygen content over the range of temperatures measured (Table II). In the oxygen deficient samples the presence of Mn(III)-O-Mn(IV) sites reduces the activation energy substantially. However, the XAS results indicate that the Mn(III) sites are located near oxygen vacancies. Worledge *et al.*[24] have found an adiabatic small polaron hopping conductivity of the form $\sigma=(A/T)e^{-Ea/kT}$ (or $\rho=T/Ae^{Ea/kT}$) to adequately describe the resistivity of the $La_{1-x}Ca_xMnO_3$ system for $x=0-1.0$ in the range 300–1000 K. The results presented here for the $\delta=0$ sample follow the same form at the temperatures studied, however, the $\delta\neq 0$ materials deviate strongly at lower temperatures. There is a change in the slope of the $\log_{10}\rho$ versus $1/T$ plot in the 60–80 K range for the $\delta=0.11$ sample (Fig. 3). This anomaly in the resistivity could be related to the turnover in the magnetic susceptibility seen near the same temperature (Fig. 4).

Magnetic properties. Figure 4 shows the magnetization (M) as a function of temperature of the samples studied. Between 150 K and room temperature, M follow the Curie-Weiss law $\chi=C/(T-\theta_p)$ (where a linear $\chi=M/H$ has been assumed). The Weiss constants θ_p are large and negative for all of these phases, indicating AF interactions (Table III). As noted previously,[25] the magnitude of the θ_p parameter, even

TABLE II. Electrical properties of $CaMnO_{3-\delta}$.

Composition	E_a (10^{-2} eV)	E_a (10^{-2} eV)
$CaMnO_3$	7.07 (above 80 K)	
$CaMnO_{2.94}$	3.38 (above 65 K)	2.46 (below 65 K)
$CaMnO_{2.89}$	2.20 (above 60 K)	1.33 (below 60 K)

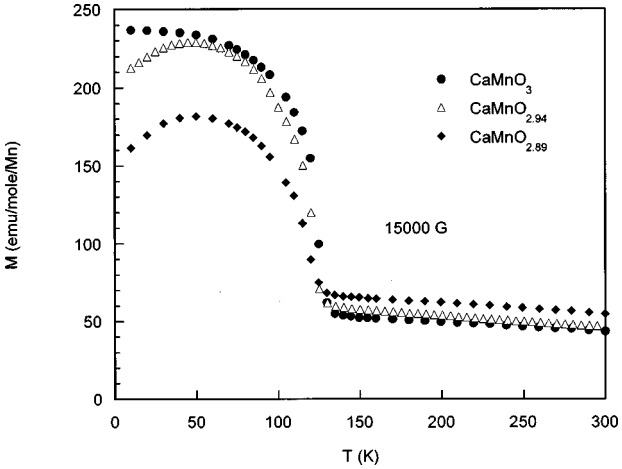

FIG. 4. Magnetization as a function of temperature for $CaMnO_{3-\delta}$.

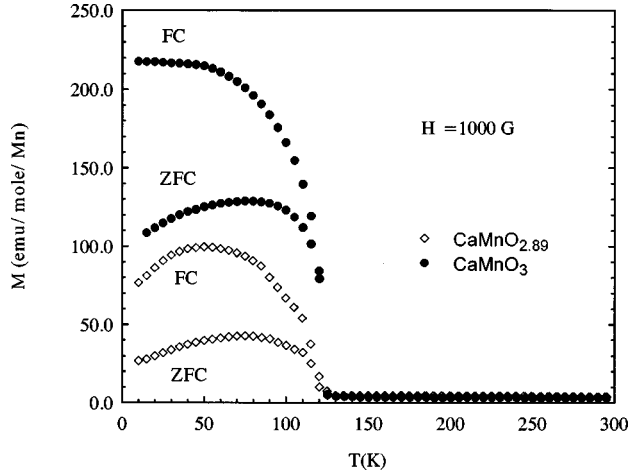

FIG. 5. Zero field and field cooled magnetization as a function of temperature for $CaMnO_{3-\delta}$.

in the $\delta=0$ material, is too high to be explained by *G*-type AF interactions. In $CaMnO_{3-\delta}$ the O-Mn-O angle is 158° (not 180° as in the ideal perovskite structure). This distortion leads to AF order at 125 K, which exhibits spontaneous or low field spin canting and hence a weak FM component. The Curie constants (*C*) are larger than the expected values and increase with decreasing oxygen content (Table III). This is attributed to the occurrence of Mn(III)-Mn(IV) clusters with a ferromagnetic intracluster interaction.[15] Again, however, the continued large θ_p values do not evidence a longer range FM component.

The local maxima in the $M(T)$ curves of the O-deficient materials motivate consideration of magnetic frustration effects such as seen in spin-glass or mictomagnetic systems. In Fig. 5 the field-cooled (FC) and zero-field-cooled (ZFC) magnetization behavior of the $\delta=0$ and 0.11 materials both show disparities. Specifically the ZFC for the fully oxygenated $CaMnO_3$ first increases then tracks the FC curve decreasing, as the temperature is raised. A similar, but larger effect is seen in the O-defect materials (Fig. 5). Such behavior is seen in spin glass and mictomagnetic (concentrated spin-glass type materials) systems where it is attributed to magnetic frustration introduced by random competing magnetic interactions. Although it is reasonable that such effects may be present in the O-deficient materials, their rather robust persistence in the fully oxygenated material makes such an explanation more difficult. An alternate interpretation, based on irreversible AF domain spin canting effects, is preferred at present.

The fact that the (FC) magnetization of this *G*-type AF material manifests a FM type increase below T_N indicates field-induced spin canting in the AF phase aided by the spontaneous canting moment. The absence of an AF peak in the susceptibility at T_N indicates that the anisotropy energy, holding the spins along the preferred direction, must have a low barrier for spin canting away from this direction. At $T=0$ K a ZFC ceramic $CaMnO_3$ sample will have many domains with random orientations of the AF easy axes. When the field is increased, those domains for which the AF polarization is perpendicular to the field, for which the canting perpendicular susceptibility is large, will dominate the magnetic response. As the temperature is increased, the AF order parameter decreases, and some domains will reorient to an axis perpendicular to the applied field, thereby yielding an increasing magnetization with increasing temperature. Eventually (with increasing *T*), most of the domains will be reoriented and the decreasing AF order parameter will yield smaller static spins to be canted, thereby leading to a decreasing magnetization with increasing temperature. This is consistent with the broad maximum observed in the ZFC magnetization vs temperature $\delta=0$ curve in Fig. 5.

In the FC case the AF domains develop below T_N with their AF polarization axes as close as possible to the transverse polarization and with their canted moment parallel with *H*. Thus the domains grow with the energetically favorable orientation of the high spin canting perpendicular susceptibility. The increasing temperature FC magnetization ($\delta=0$) therefore manifests only the weakening transverse response that accompanies the AF order parameter decrease (i.e., no maximum occurs as the domains were grown transverse).

In the O-deficient material the ZFC magnetization is still more strongly suppressed at $T=0$. Moreover in the $\delta=0.11$ material even the FC magnetization exhibits a local maximum (as do the $H=15$ kOe curves in Fig. 4). This would be consistent with the Mn(III)-O-Mn(IV) clusters having their net spin aligned with the overall AF polarization axis. In an external field, the preferred alignment of these clusters would be along the external field direction. Thus the clusters would hinder the field-induced transverse reorientation of the AF domains thereby increasing the low-*T* down turn in magnetization, due to incomplete transverse polarization. The suppression of the small spontaneous canting (at $H=0$) in the O-deficient materials probably also occurs. Moreover, the breaks in the slope of the FC magnetization of the $\delta=0.11$

TABLE III. Magnetic properties of $CaMnO_{3-\delta}$.

Composition	T_N (K)	C (emu/mol K)	μ_{eff}	θ_p (K)
$CaMnO_3$	125	2.25	4.24	−472
$CaMnO_{2.94}$	125	2.46	4.44	−494
$CaMnO_{2.89}$	125	2.99	4.89	−462

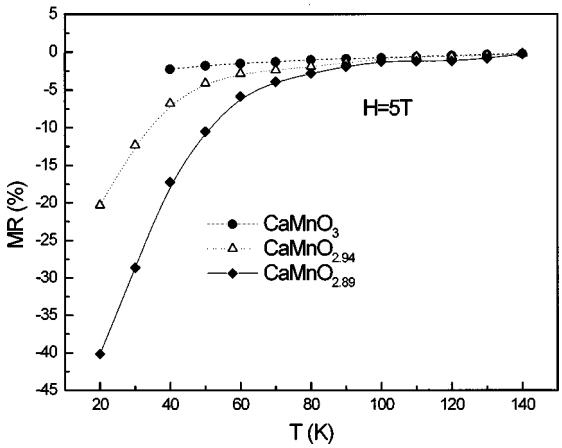

FIG. 6. MR as a function of temperature for $CaMnO_{3-\delta}$.

material may indicate actual reorientation phase transitions.

Magnetoresistance. The magnetoresistance is defined as $MR=(\rho_H-\rho)/\rho_0$, where ρ_H and ρ are the resistivities at H and zero applied magnetic field. Figure 6 shows the MR as a function of temperature for the $CaMnO_{3-\delta}$ materials. A negative MR effect is observed below the T_N. However, MR of $CaMnO_3$ is negligible. The concentration of Mn(III) increases with decreasing oxygen content and with it the possibility of local double exchange. The MR is, however, not related to that seen at the paramagnetic-ferromagnetic–semiconductor-metal transition in double exchange materials, where the MR is sharply peaked around T_c. The MR here is more analogous to GMR materials where the MR grows with the AF order parameter below T_N.[26] In the GMR materials the field flips selected spin layers. In these $CaMnO_{3-\delta}$ materials AF domain reorientation appears to be important below T_N. The O vacancies appear to substantially modify these domain effects. The MR could therefore be related to AF domain scattering effects (somewhat reminiscent of GMR materials). Further work is clearly required to establish the exact mechanism of MR in $CaMnO_{3-\delta}$.

CONCLUSIONS

Titration and Mn-K XAS indicate the reduction of Mn(IV) to Mn(III) with increasing δ in the $CaMnO_{3-\delta}$ system by the creation of two five coordinate Mn(III) sites per O vacancy. The resistivity of the electron doped $CaMnO_{3-\delta}$ decreases as δ increases but remains semiconducting in the range 20–300 K. The superexchange interactions that lead to G-type antiferromagnetic ordering in the $\delta=0$, Mn(IV) material still dominate in the O-defect materials, however, the AF-domain canting appears hindered. Evidence of FM intracluster Mn(IV)-O-Mn(IV) interactions are found in the Curie constant enhancement with increasing δ. A large ~40% MR is demonstrated in $CaMnO_{2.89}$.

ACKNOWLEDGMENTS

The authors thank Professor K. V. Ramanujachary and Dr. J. E. Sunstrom IV for their suggestions with experimental problems and useful discussions. The ICP analysis was carried out in the Chemistry Department of Rider College with the help of Dr. W. H. McCarroll. This work was supported by National Science Foundation-Solid State Chemistry Grant Nos. DMR-93-14605 and DMR-96-13106.

*Electronic address: martha@rutchem.rutgers.edu

[1] K. Chahara, T. Ohno, M. Kasai, and Y. Kozono, Appl. Phys. Lett. **63**, 1990 (1993).
[2] R. von Helmolt, J. Wocker, B. Holzapfel, M. Schultz, and K. Samwer, Phys. Rev. Lett. **71**, 2331 (1993).
[3] S. Jin, T. H. Tiefel, M. McCormack, R. A. Fastnacht, R. Ramesh, and L. H. Chen, Science **264**, 413 (1994).
[4] H. L. Ju, C. Kwon, R. L. Greene, and T. Venkatesan, Appl. Phys. Lett. **65**, 2108 (1994).
[5] M. McCormack, S. Jin, T. H. Tiefel, R. M. Fleming, and J. M. Phillips, Appl. Phys. Lett. **64**, 3045 (1994).
[6] S. Sundar Manoharan *et al.*, J. Appl. Phys. **76**, 3923 (1994).
[7] R. Mahendiran, R. Mahesh, A. K. Raychaudhuri, and C. N. Rao, J. Phys. D **28**, 1743 (1995).
[8] T. Shimura, T. Hayashi, Y. Inaguma, and M. Itoh, J. Solid State Chem. **124**, 250 (1996).
[9] P. M. Levy, Science **256**, 972 (1992).
[10] E. O. Wollan and W. C. Koehler, Phys. Rev. **100**, 545 (1955).
[11] J. Töpfer and J. B. Goodenough, J. Solid State Chem. **130**, 117 (1997).
[12] J. A. Alonso, M. J. Martinez-lope, M. T. Casais, and A. Munoz, Solid State Commun. **102**, 7 (1997).
[13] A. Maignan, C. Michel, M. Hervieu, and B. Raveau, Solid State Commun. **101**, 277 (1997).
[14] W. H. McCarrol, K. V. Ramanujachary, and M. Greenblatt, Solid State Chem. **136**, 322 (1998).
[15] J. Briatico, B. Alascio, R. Allub, A. Butera, A. Laneiro, M. T. Causa, and M. Tovar, Phys. Rev. B **53**, 14 020 (1996).
[16] H. Tagachi, Phys. Status Solidi A **88**, K79 (1985).
[17] M. Croft, D. Sills, M. Greenblatt, C. Lee, S-W. Cheong, K. V. Ramanujachary, and D. Tran, Phys. Rev. B **55**, 8726 (1997).
[18] A. Sahiner, M. Croft, S. Guha, I. Perez, Z. Zhang, M Greenblatt, P. Metcalf, H. Jahns, and G. Liang, Phys. Rev. B **51**, 5879 (1995).
[19] A. Sahiner, M. Croft, S. Guha, Z. Zhang, M. Greenblatt, I. Perez, P. Metcalf, H. Jahns, G. Liang, and Y. Seon, Phys. Rev. B **53**, 9745 (1996).
[20] K. R. Poeppelmeier, M. E. Leonowicz, J. C. Scanlon, and J. M. Longo, J. Solid State Chem. **45**, 71 (1982).
[21] See E. Paris *et al.*, Physica B **208/209**, 351 (1995).
[22] M. Croft and M. Greenblatt (unpublished).
[23] R. D. Shannon, Acta Crystallogr., Sect. A: Cryst. Phys., Diffr., Theor. Gen. Crystallogr. **32**, 751 (1976).
[24] D. C. Worledge, L. Mieville, and T. H. Geballe, Phys. Rev. B **57**, 15 267 (1998).
[25] I. D. Fawcett, J. E. Sunstrom IV, M. Greenblatt, M. Croft, and K. V. Ramanujachary, Chem. Mater. **10**, 3643 (1998).
[26] X. Barthelemy, A. Fert, M. N. Baibich, S. Hadjioudj, F. Petroff, P. Etienne, R. Cabanol, S. Lequien, F. Nguyen Van Dau, and G. Creuzet, J. Appl. Phys. **67**, 5908 (1990).